TIP47 functions in the biogenesis of lipid droplets

Anna V. Bulankina,[1] Anke Deggerich,[3,4] Dirk Wenzel,[5] Kudzai Mutenda,[1] Julia G. Wittmann,[2] Markus G. Rudolph,[2] Koert N.J. Burger,[6] and Stefan Höning[3,4]

[1]Institute for Biochemistry II and [2]Department of Molecular Structural Biology, University of Göttingen, 37073 Göttingen, Germany
[3]Institute for Biochemistry I and [4]Cologne Center for Molecular Medicine, University of Cologne, 50931 Cologne, Germany
[5]Department of Neurobiology, Max-Planck Institute for Biophysical Chemistry, 37077 Göttingen, Germany
[6]Section Endocrinology and Metabolism, Faculty of Science and Institute of Biomembranes, Utrecht University, 3584 CH Utrecht, Netherlands

TIP47 (tail-interacting protein of 47 kD) was characterized as a cargo selection device for mannose 6-phosphate receptors (MPRs), directing their transport from endosomes to the trans-Golgi network. In contrast, our current analysis shows that cytosolic TIP47 is not recruited to organelles of the biosynthetic and endocytic pathways. Knockdown of TIP47 expression had no effect on MPR distribution or trafficking and did not affect lysosomal enzyme sorting. Therefore, our data argue against a function of TIP47 as a sorting device. Instead, TIP47 is recruited to lipid droplets (LDs) by an amino-terminal sequence comprising 11-mer repeats. We show that TIP47 has apolipoprotein-like properties and reorganizes liposomes into small lipid discs. Suppression of TIP47 blocked LD maturation and decreased the incorporation of triacylglycerol into LDs. We conclude that TIP47 functions in the biogenesis of LDs.

Introduction

The transport of lysosomal enzymes from the TGN to endosomes depends mainly on the two mannose 6-phosphate receptors (MPRs), MPR46 or MPR300. The hydrolases are delivered to lysosomes after pH-induced dissociation of the enzyme receptor complexes in endosomes, whereas the MPRs cycle back to the TGN (Bonifacino and Rojas, 2006). A protein shown to be involved in retrograde trafficking of MPRs from endosomes is TIP47 (tail-interacting protein of 47 kD). A current model suggests that GTP-bound Rab9 binds cytosolic TIP47 and promotes its interaction with the cytoplasmic tail of MPRs, thereby initiating retrograde trafficking of the receptors (Carroll et al., 2001).

In addition to its function as a cytoplasmic sorting factor, TIP47 is found associated with lipid droplets (LDs; Wolins et al., 2001; Miura et al., 2002; Than et al., 2003). LDs are composed of a neutral lipid core, mainly triacylglycerol (TAG) and cholesterol esters, covered with a phospholipid-cholesterol monolayer and associated proteins (Tauchi-Sato et al., 2002). TIP47, among other proteins, decorates the LD hemimembrane (Miura et al., 2002). Indeed, TIP47 was also identified as a placental protein that exhibits 43% sequence identity with adipose differentiation-related protein (ADRP; also named Adipophilin), a ubiquitously expressed protein and known component of LDs (Than et al., 1998). Together with Perilipin, ADRP and TIP47 are the founding members of the family of LD-associated PAT (Perilipin, Adipophilin, and TIP47) proteins, which also includes S3-12 and OXPAT (Brasaemle, 2007). Perilipin is the best-studied member and a key regulator of lipolysis (Tansey et al., 2003), whereas the precise functions of S3-12, OXPAT, TIP47, and ADRP remain ill defined.

We show in this study that TIP47 does not colocalize with MPRs, Rab9, and marker proteins of the biosynthetic and endocytic pathways. The reported nucleotide-dependent binding of Rab9 to TIP47 could not be confirmed. Our results demonstrate that cytosolic TIP47 was recruited to LDs in all cell types analyzed, and the amino acid sequence 87–198 of TIP47 was sufficient for targeting GFP to the LD surface. Knockdown (KD) of TIP47 did not disturb the localization,

A.V. Bulankina and A. Deggerich contributed equally to this paper.

Correspondence to S. Höning: shoening@uni-koeln.de

A.V. Bulankina's present address is InnerEarLab, Dept. of Otolaryngology and Center for Molecular Physiology of the Brain, University of Göttingen, 37075 Göttingen, Germany.

K. Mutenda's present address is Dept. of Biochemistry and Molecular Biology, University of Southern Denmark, 5230 Odense M, Denmark.

Abbreviations used in this paper: ADRP, adipose differentiation-related protein; apoE, apolipoprotein E; CatD, cathepsin D; DMPC, dimyristoyl-phosphatidylcholine; KD, knockdown; LD, lipid droplet; MPR, mannose 6-phosphate receptor; PNS, postnuclear supernatant; SPR, surface plasmon resonance; TAG, triacylglycerol.

The Rockefeller University Press $30.00
J. Cell Biol. Vol. 185 No. 4 641–655
www.jcb.org/cgi/doi/10.1083/jcb.200812042

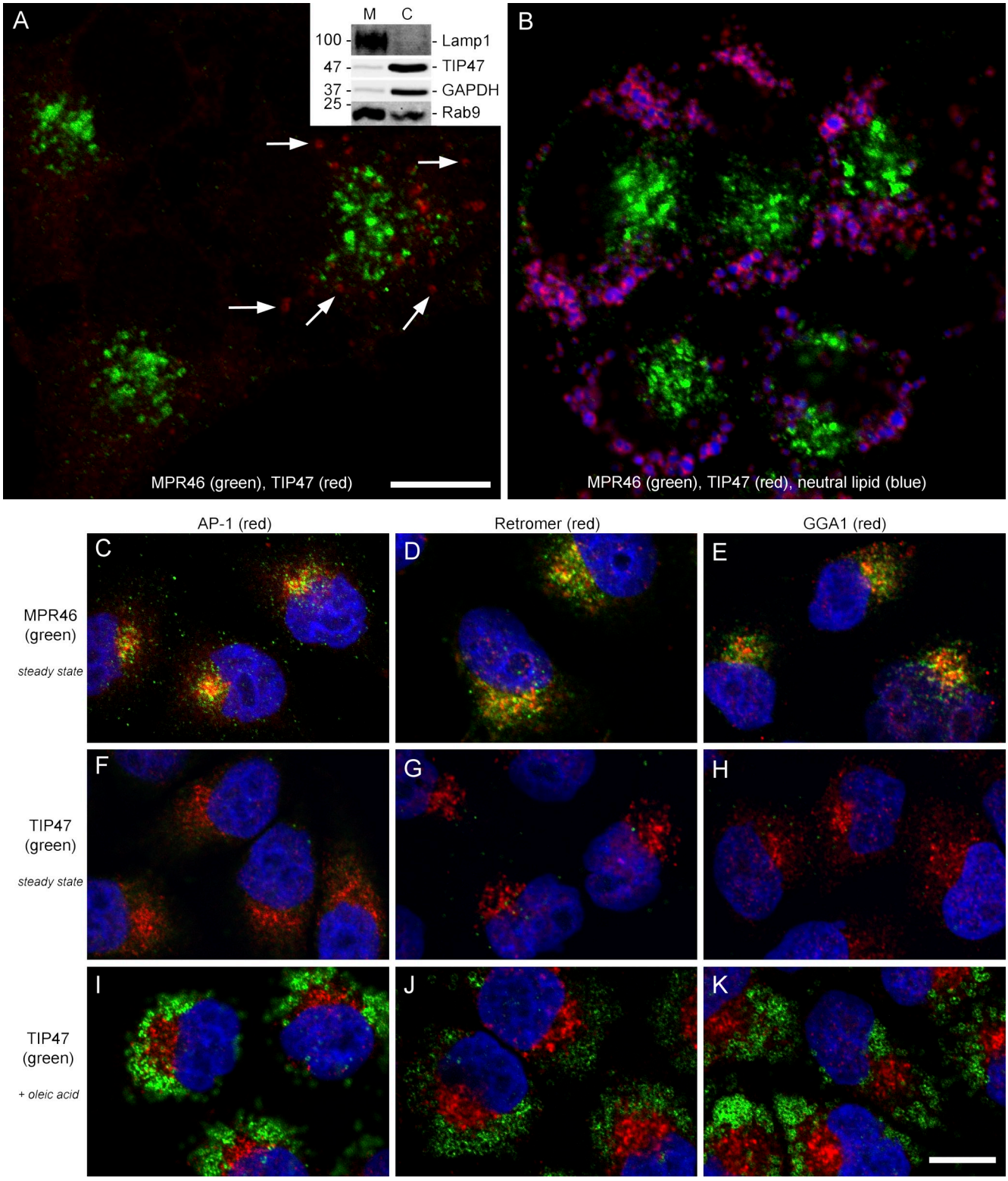

Figure 1. **TIP47 and MPR46 localize to different compartments.** (A and B) Staining of HeLa cells for MPR46 (green), TIP47 (red), and neutral lipid (blue) at steady state (A) or after oleic acid feeding (B). Arrows point to small TIP47-positive structures. (inset) Western blot for the indicated proteins after fractionation of cells into membranes (M) and cytosol (C). Values are shown in kilodaltons. (C–K) Staining of MPR46, TIP47, and the indicated sorting proteins in HeLa cells at steady state (C–H) or after oleic acid feeding (I–K). Colocalization is indicated in yellow. Bars, 15 µm.

trafficking, or function of MPRs. In contrast, the biogenesis of LDs was altered, and the incorporation of newly synthesized TAG into LDs diminished. Most notably, recombinant TIP47 behaved as the classical apolipoprotein E (apoE), reorganizing dimyristoyl-phosphatidylcholine (DMPC) liposomes into small 23-nm discs.

Results

TIP47 is recruited to LDs

To analyze MPR sorting, we attempted to use TIP47 as a marker for an endosomal subpopulation from which MPRs return to the TGN. We expected significant colocalization of TIP47 and MPRs, but all attempts to detect TIP47 on structures that were labeled with MPR46 (Fig. 1 A) or MPR300 (not depicted) in immunofluorescence failed. Actually, TIP47 was almost undetectable in HeLa cells at steady state, and only a low percentage of cells showed TIP47 staining of dot-like structures (Fig. 1 A, arrows). Consistent with these observations, biochemistry revealed that TIP47 is mostly cytosolic in contrast to Rab9, which distributes to membranes and the cytosol (Fig. 1 A, inset).

We then cultivated HeLa cells for 16 h in medium with oleic acid complexed to BSA before fixation to induce LD formation. TIP47 became easily detectable in every cell on the surface of LDs, which were unequivocally identified by incorporation of a neutral lipid dye or labeling with ADRP (Figs. 1 B, S1, S2, and S4), but no colocalization with MPR46 was evident. Identical results were obtained in all cells of all species tested (Fig. S1). These observations suggest that the intracellular localization is not cell type specific.

If TIP47 acts as a sorting factor for MPRs (Diaz and Pfeffer, 1998; Carroll et al., 2001), the lack of TIP47 localization on structures containing these receptors is surprising. Other components of the intracellular cytoplasmic sorting machinery colocalize to some extent with their cargo, other sorting factors, or organelle markers (Puertollano et al., 2001; Ghosh et al., 2003; Arighi et al., 2004). AP-1, GGA1, and retromer, which also mediate MPR trafficking, were all detected in close apposition to MPRs and partially overlapped with them (Fig. 1, C–E, MPR46). In contrast, TIP47 staining was distinct from factors of the sorting machinery tested (Fig. 1, F–K), irrespective of whether cells were fixed at steady state or after oleic acid feeding. This either indicates a low affinity for those organelles, or it suggests that TIP47 cannot be regarded as a typical sorting factor of MPRs. In line with the latter assumption, it was impossible to detect TIP47 on organelles of the endocytic and the biosynthetic pathways (Fig. S2).

The lack of TIP47 labeling on organelles involved in membrane protein sorting may be the result of questionable antibody specificity (Barbero et al., 2001; Wolins et al., 2001), but all antibodies against TIP47 available to us detect a single protein when analyzed by Western blotting and/or immunoprecipitation (Fig. S3) and gave identical immunofluorescence staining patterns. To further corroborate TIP47 localization, we generated GFP- or short peptide–tagged TIP47 chimeras and transfected them into HeLa cells. The fusion proteins decorated neutral lipid-positive LDs and colocalized with ADRP but not with MPR46 (Fig. S4). Thus, we conclude that TIP47 is not recruited to organelles of the biosynthetic and endocytic pathways but specifically decorates LDs, which is in line with earlier observations (Wolins et al., 2001; Miura et al., 2002, Than et al., 2003; Robenek et al., 2005).

TIP47 does not interact with Rab9

The putative binding of TIP47 to MPRs is thought to depend on activated (GTP bound) Rab9. We therefore analyzed the subcellular localization of endogenous TIP47 and Rab9 in HeLa cells. The Rab9 staining pattern was distinct from TIP47, and only a minor fraction of MPR46 was detectable in Rab9-positive structures (Fig. 2). Consistent with the notion that Rab9 decorates late endosomes, we observed colocalization with GFP-Rab7 and GFP-Lamp1 (Falcon-Perez et al., 2005). In cells in which TIP47 was detectable in small dot-like structures at steady state (presumably nascent LDs), it was still undetectable on Rab9-positive late endosomes (Fig. 2, inset). One may argue that TIP47 escapes detection because only a minor fraction of the protein is recruited to membranes at any time. To address this issue, we expressed CFP/YFP fusions of Rab9, TIP47, and ADRP to verify their subcellular localization. Again, CFP-Rab9 localized to vesicles distributed throughout the cytoplasm at steady state (Fig. 3, B and C) and after oleic acid feeding (Fig. 3, F and G). YFP-TIP47 displayed a diffuse cytoplasmic staining at steady state irrespective of the expression level, which varied by a factor of eight as analyzed by fluorescence intensity profile scans (compare Fig. 3, A, C, and D). After oleic acid feeding, YFP-TIP47 decorated the surface of LDs with a significant degree of colocalization with CFP-ADRP (Fig. 3 H), whereas the staining patterns of CFP-Rab9 and YFP-TIP47 remained completely separated (Fig. 3 G). Identical results were obtained in cells expressing YFP-TIP47 and

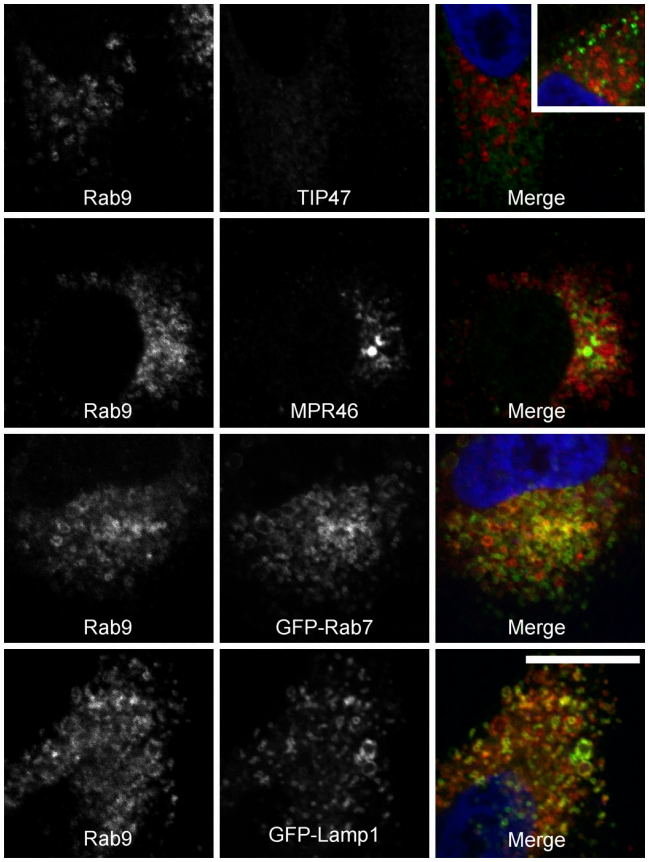

Figure 2. **Endogenous TIP47 and Rab9 do not colocalize.** HeLa cells were fixed and stained for the indicated proteins. GFP-Rab7 and GFP-Lamp1 were transiently transfected 48 h prior to fixation. Colocalization is indicated in yellow. The inset displays a cell with small LDs at steady state. Bar, 15 μm.

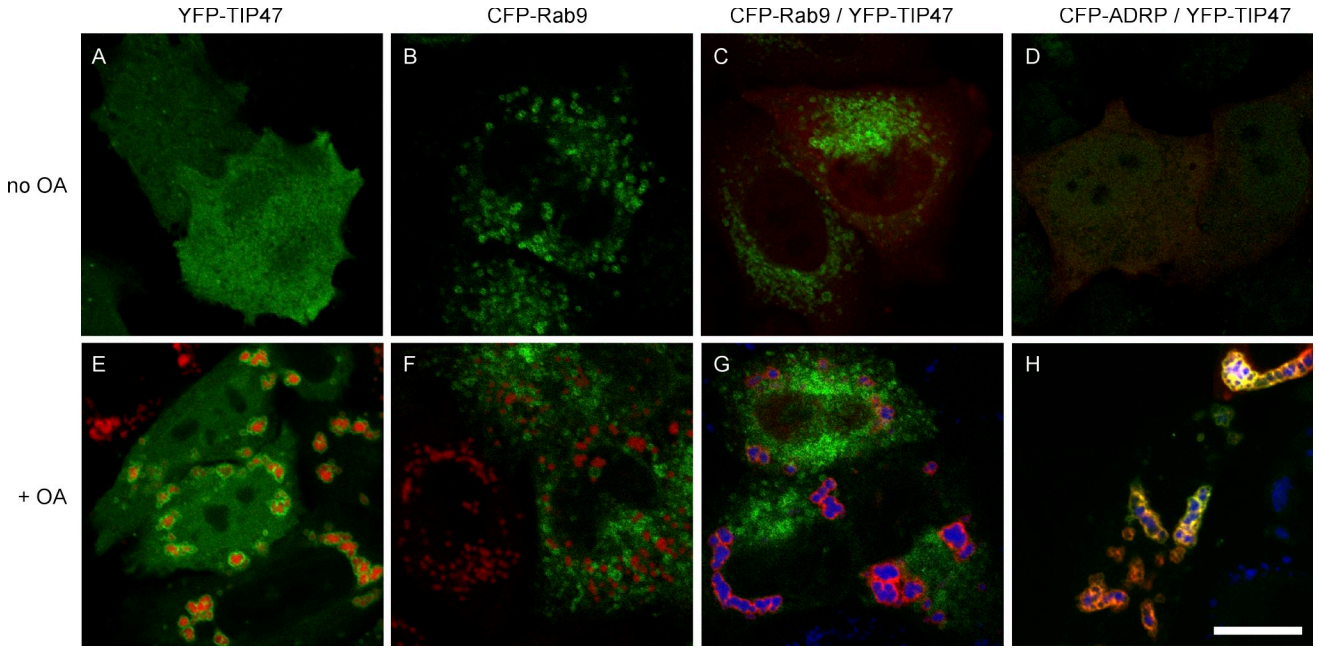

Figure 3. **CFP-Rab9 does not colocalize with YFP-TIP47.** (A–H) HeLa cells were transiently transfected with YFP-TIP47 (A and E, green), CFP-Rab9 (B and F, green), CFP-Rab9, and YFP-TIP47 (C and G; green, CFP; red, YFP) or with CFP-ADRP and YFP-TIP47 (D and H; green, CFP; red, YFP). Cells depicted in the bottom panels were fixed after oleic acid (OA) feeding. A neutral lipid stain is shown in red (E and F) or blue (G and H). Brightness and contrast of TIP47 staining in A and E were enhanced to visualize the otherwise faint cytoplasmic staining. Colocalization is indicated in yellow. Bar, 15 µm.

CFP fusions of either the GTP- or GDP-locked mutants of Rab9 (Rab9 Q66L and Rab9 S21N; unpublished data).

These findings are inconsistent with the reported binding of Rab9 to TIP47. To verify a direct interaction between TIP47 and Rab9 (Carroll et al. 2001), we analyzed the nucleotide-dependent interaction of recombinant TIP47 and Rab9 in vitro. First, pull-down assays were performed using His_6-GST-TIP47 with Rab9 either complexed to GDP, GTP, or the nonhydrolysable GTP analogue GppNHp. GTP was used in addition to GppNHp to exclude any possible influence of the nature of the nonhydrolysable nucleotide on the binding event. To test the stability of the Rab9–GTP complex, the Rab9-catalyzed GTP hydrolysis was followed at 25°C and yielded a half-life of 6.7 h, which is long enough to ensure a high amount of Rab9–GTP complex during the time course of the pull-down assays. In all cases, Rab9 was not retained by TIP47 (Fig. 4 A). Likewise, analytical gel filtration of TIP47 with either Rab9–GTP or Rab9–GppNHp resulted in separate elution of these proteins, and no additional peaks that might represent TIP47–Rab9 complexes could be detected (Fig. 4 B).

Previously, KD of TIP47 was shown to result in increased cytosolic Rab9 and shifting of the cytosol to membrane ratio of the remaining TIP47 toward membranes (Ganley et al., 2004). In this study, KD of TIP47 had no effect on the cytosol to membrane ratio of Rab9. In control cells, TIP47 was predominantly cytosolic, and the membrane fraction decreased to below the limit of detection in TIP47 RNAi cells (Fig. 4 C). Even transfection of cells with wild-type, GTP-locked, or GDP-locked Rab9 had no effect on the cytosolic localization of TIP47 (unpublished data). This shows that neither ectopic expression nor KD of Rab9 affect TIP47 expression or its intracellular distribution. We also used immunoprecipitation of TIP47 to test for association with Rab9, but no Rab9 was recovered, even under mild washing conditions (Fig. 4 D). Finally, TIP47 was used as bait to test for binding to GTP- or GDP-locked forms of 32 different Rab proteins in a yeast two-hybrid screen. However, no specific interaction was identified (unpublished data). Thus, we are sceptical that TIP47 is a physiologically relevant direct binding partner of Rab9.

RNAi of TIP47 does not affect MPR trafficking and function

We next analyzed the intracellular distribution and function of MPRs in the absence of TIP47 using an RNAi-based approach. The subcellular localization of MPR300 at steady state in TIP47 RNAi cells was comparable with the controls (Fig. 5, A and C), whereas KD of Vps35/26 caused a more disperse localization of the receptor (Fig. 5 E). The defects in MPR300 sorting in Vps35/26 KD cells became more evident when the cells were allowed to internalize antibodies against the lumenal receptor domain. Although the antibodies were delivered to the Golgi region of control and TIP47 KD cells, they were retained in peripheral endosomal structures of Vps35/26 KD cells (Arighi et al., 2004; Seaman 2004). Similar results were obtained for MPR46, although the endosomal retention was less pronounced. Thus, suppression of TIP47 does not cause trafficking defects of MPR300 or MPR46.

We then analyzed whether TIP47 RNAi affect the turnover of MPR300. Cells were incubated in the absence or presence of cycloheximide followed by preparation of total cell extracts and detection of MPR300 in Western blots (Fig. 6 A). In an alternative approach, we used receptor immunoprecipitation after

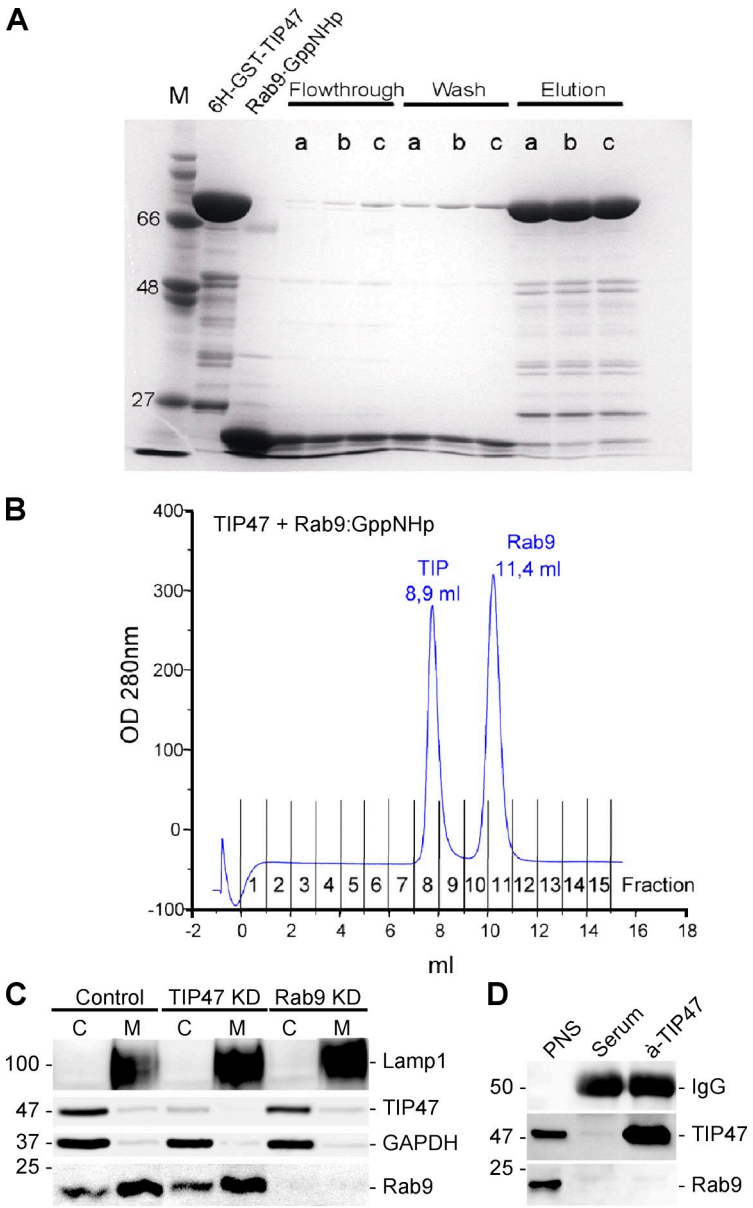

Figure 4. **TIP47 does not bind to Rab9 in vitro.** (A) Pull-down assay is shown. His_6-GST-TIP47 was loaded on beads, and Rab9 either complexed to GDP (lanes a), GTP (lanes b), or GppNHp (lanes c) was added in equimolar amounts. After 2 h, the flow through and the wash fractions were collected before the beads were eluted. All fractions were analyzed by SDS-PAGE. The first two lanes show free His_6-GST-TIP47 and Rab9 for size comparison. M, marker. (B) Analytical gel filtration of an equimolar mixture of TIP47 and Rab9 complexed to GppNHp that had been incubated for 2 h. (C) Western blot detection of the indicated proteins in cytosol (C) and membranes (M) from control (HeLa), TIP47 KD, and Rab9 KD cells. (D) Detection of the indicated proteins in immunoprecipitates of a nonspecific serum or a TIP47-specific rabbit serum. An aliquot (1%) of a PNS served as a control for the protein detection. Values on blots are shown in kilodaltons.

pulse-chase labeling (Fig. 6 B). Both assays showed that loss of TIP47 does not affect MPR300 turnover. To validate the function of MPRs in TIP47 KD cells, we analyzed the sorting and maturation of the lysosomal hydrolase cathepsin D (CatD). After 6 h of incubation, cells and their culture supernatants were collected and processed for the detection of CatD. In control and TIP47 KD cells, the 27-kD mature form of CatD was predominant, whereas the 50-kD precursor and the intermediate form represented minor fractions. As expected, the culture supernatants contained just small amounts of the secreted CatD precursor. In sharp contrast, the intracellular mature form of CatD was decreased in Vps35/26 KD cells, and massive amounts of the enzyme precursor were secreted (Fig. 6 C), which is in agreement with earlier observations (Seaman, 2004; Perez-Victoria et al., 2008). Similar results were obtained with enzyme activity assays for β-hexosaminidase (unpublished data), thus confirming that KD of TIP47 does not affect MPR-dependent sorting of lysosomal enzymes.

To directly assay binding of TIP47 to MPRs, we immobilized GST fusion proteins of both full-length MPR cytoplasmic tail sequences on a CM5 sensor surface of a surface plasmon resonance (SPR) biosensor. The MPR tail fragments were then probed for the binding of recombinant TIP47 and control proteins. As shown in Fig. 6 E, the MPR300 tail bound to GGA1-VHS (Vsp27p/Hrs/STAM domain) as well as to AP2 but not to GST. Binding of TIP47 was only marginally above the nonspecific background. Identical results were obtained with the immobilized tail of MPR46 (unpublished data). Both MPR tail sequences were immobilized at very high densities, and three different buffer systems were applied for the binding experiments. However, even high concentrations of TIP47 (25 μM) were not sufficient to record a specific interaction with the MPR cytoplasmic tails. In summary, we are not able to convincingly demonstrate that MPRs bind TIP47 or that MPR distribution, trafficking, and function require TIP47.

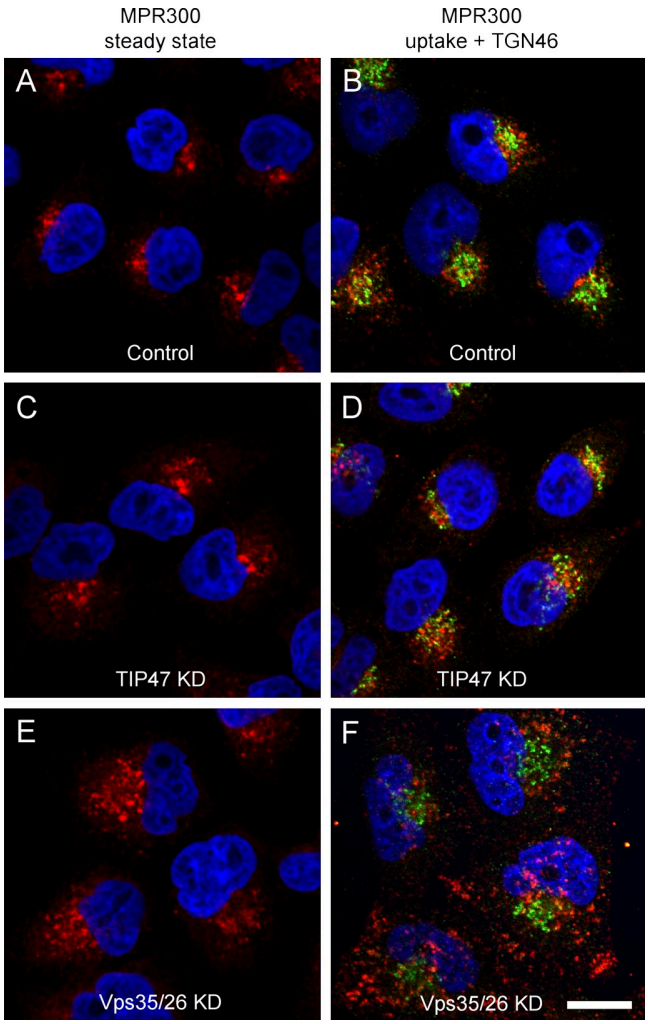

Figure 5. **TIP47 KD does not affect MPR localization and endocytosis.** (A–F) Mock-transfected HeLa cells (control; A and B), TIP47 KD (C and D), and Vps35/26 KD cells (E and F) were either stained for MPR300 (red) at steady state (A, C, and E) or allowed to internalize anti-MPR300 antibodies (B, D, and F) before fixation and detection of uptake (red) and staining of TGN46 (green). Colocalization is indicated in yellow. The RNAi efficiency is shown in Fig. 6 D. Bar, 15 µm.

TIP47 is recruited to newly forming LDs

We noticed that the number of LDs detectable at steady state varied depending on cell type. Although LDs were abundant in some cell lines (HepG2, HuH-7, CHO, and Cos-7), most HeLa cells lack LDs at steady state and show no staining of TIP47. However, TIP47 was detectable on the surface of LDs in a few cells. LDs disappeared after starvation in culture medium with low serum (2% overnight; Fig. S3). When starved cells were incubated in the presence of oleic acid, the first small TIP47-positive structures appeared within 5–10 min, but these structures were not stained by a neutral lipid dye. Within time, the number of TIP47-positive structures increased, they became larger in size, and were brightly stained by neutral lipid dyes (see Fig. S5 for time course). After 24 h of oleic acid feeding, LDs had diameters up to 2 µm. Droplets of an equivalent size were detectable in living cells incubated with a neutral lipid dye alone or in cells expressing GFP-TIP47. The time course of TIP47 recruitment fits well to the formation of LDs in living cells as analyzed by two-photon microscopy with fluorescent polyene lipids (Kuerschner et al., 2008). We noticed that LDs of HepG2 cells contained ADRP but not TIP47 at steady state. However, shortly after fatty acid feeding, the newly forming small nascent LDs were labeled by TIP47 (unpublished data). We conclude that TIP47 may have a function early in the biogenesis of LDs.

The 11-mer repeat region of TIP47 is sufficient for LD targeting

Perilipin, ADRP, and TIP47, the core members of the PAT family of proteins (Miura et al., 2002), share ∼40% identity in their N-terminal 120 amino acids (Brasaemle, 2007). However, it is unclear whether they are recruited to LDs in a conserved way. We therefore created GFP- or peptide-tagged N- and/or C-terminally truncated versions of TIP47 to further examine the association of TIP47 with LDs. Although wild-type GFP-TIP47 and the C-terminal deleted variant (Δ 210–434) were recruited to LDs (Fig. 7 A), truncation of the N-terminal half (Δ 1–198) totally abolished LD association (Fig. 7 C). Deletion of the first 86 residues (Δ 1–86) was tolerated, whereas deletion of 116 residues compromised LD recruitment. The N-terminal half of TIP47 harbors 11-mer repeats that may form amphipathic helices (Bussell and Eliezer, 2003). We therefore generated two GFP-TIP47 fragments harboring amino acid residues 56–198 or 86–198 and evaluated their LD association. Both fragments labeled the LD surface, but in contrast to wild-type GFP-TIP47, significant amounts of both fusion proteins were also detectable in the cytosol (Fig. 7 B). This may be a consequence of either massive overproduction or altered conformation. Thus, the minimal sequence information required for complete recruitment to LDs is located between residues 87–209, whereas the 11-mer repeat regions are sufficient for partial localization to LDs.

Suppression of TIP47 affects LD formation and TAG storage

We noticed that suppression of TIP47 resulted in up-regulation of its closest relative, ADRP. The protein is continually synthesized but immediately degraded in cells that lack LDs (Xu et al., 2005). The protein levels of ADRP in TIP47 RNAi cells were elevated two- to fourfold as compared with mock-transfected cells after oleic acid feeding. Likewise, more ADRP was detectable on LDs freshly isolated from TIP47 KD cells (Fig. 8 A), suggesting that ADRP may have a compensatory function in cells depleted of TIP47.

Floating LDs recovered from the top of a sucrose gradient (fraction 1; Fig. 8 B) contained up to 25% of all detectable TIP47, whereas marker proteins of the cytosol, the plasma membrane, and lysosomes were not present (Fig. 8 B). When KD cells were subjected to subcellular fractionation, TIP47 was only detectable in the top fraction. This shows that upon fatty acid feeding of RNAi cells, all remaining TIP47 is recruited to LDs, whereas the cytosolic protein pool is depleted. The change in the subcellular distribution was specific, as markers of other organelles, including the ER, Golgi, plasma membrane, and lysosomes were distributed like in the controls (unpublished data).

To gain insight into the protein composition of LDs, the freshly isolated material was washed, adjusted to equal amounts of

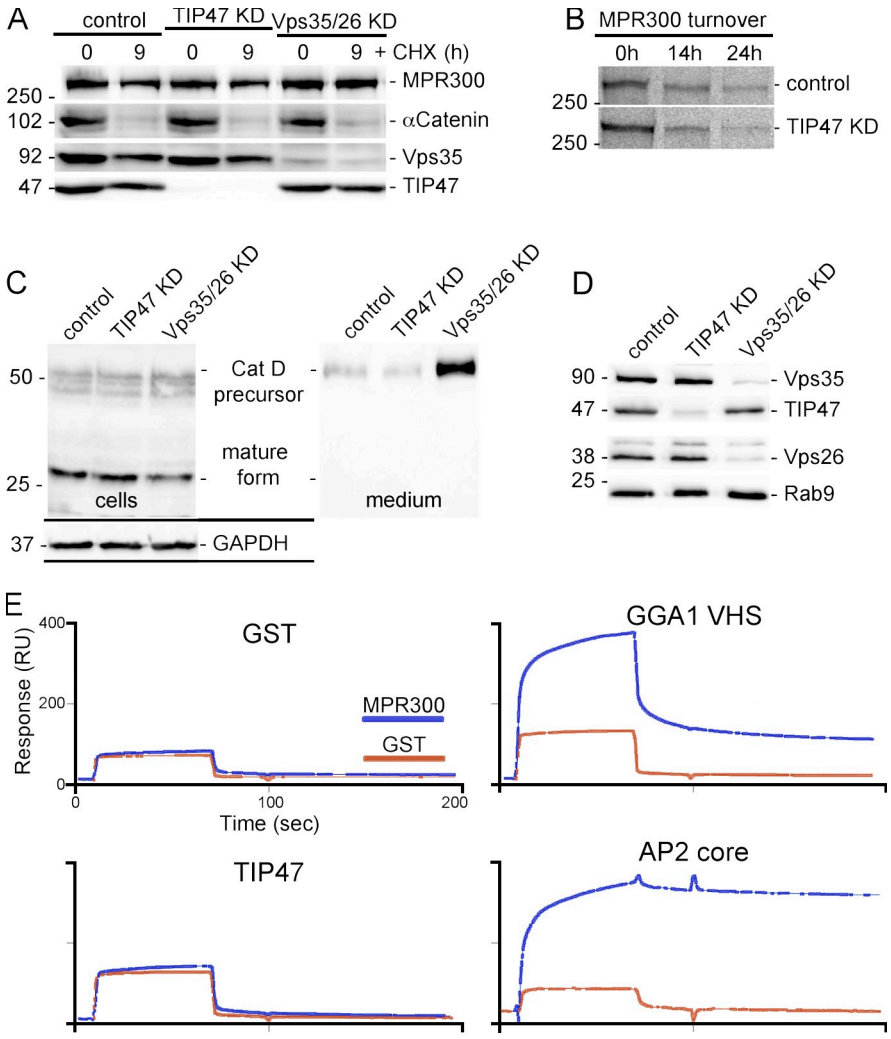

Figure 6. **TIP47 does not bind MPR300 and is dispensable for its function.** (A) Protein turnover detected in Western blots of the indicated cells incubated for 9 h in presence/absence (0 h) of cycloheximide (CHX). (B) Autoradiography of MPR300 immunoprecipitated from cells that were pulse labeled with [35S]-Met/Cys and chased for up to 24 h. (C) CatD maturation was analyzed in Western blots of cell lysates and their respective culture supernatants. (D) The KD of TIP47 and Vps35/26 was verified by Western blots. (E) GST and a GST fusion protein containing the full-length MPR300 cytoplasmic tail were coupled to a CM5 surface of a SPR biosensor and subsequently probed for the binding of the indicated proteins used at 5 μM. RU, resonance units. Values on blots are shown in kilodaltons.

protein, and subjected to SDS-PAGE and peptide mass fingerprint analysis of several prominent protein bands. Six of the major protein bands were identified as known LD-associated proteins, including ADRP, TIP47, and NAD phosphate–dependent steroid dehydrogenase (Fig. 8 C). The intensity of the ADRP-containing protein band was unchanged in LDs from TIP47 KD cells, although a Western blot of freshly isolated LDs revealed higher amounts of ADRP (Fig. 8 A). A likely explanation is that ADRP is sensitive to the washing conditions that were applied before SDS-PAGE.

After oleic acid feeding, HeLa cells contain a large number of TIP47-positive LDs scattered throughout the cytoplasm with diameters of up to 2 μm (Fig. 9 A). In TIP47 KD cells, the number of mature (large) LDs was decreased, but the remaining droplets still contained TIP47, which is in agreement with our fractionation analysis (Fig. 8 B). Quantification of the TIP47 fluorescence intensities showed a drop by 69% in the RNAi cells. Please note that this method ignores the amount of TIP47 in the cytosol and that protein KD is much higher than 69% (compare with Western blots in Fig. 6, A and D; Fig. 8 A; or Fig. 9 G). TIP47 was present on small dot-like structures in the KD cells, suggesting that the cells start to respond to fatty acid feeding with the formation of LDs, but their complete maturation is inhibited (Fig. 9 B). This notion is further supported by the quantification of neutral lipid incorporation, which showed a 59% decrease in the RNAi cells (Fig. 9, C and D). To corroborate these data, we used living cells and quantified the mean fluorescence signal intensities of the neutral lipid dye by flow cytofluorometry (Fig. 9 E). The staining in TIP47 RNAi cells was reduced by 35%, confirming the inhibition of TAG storage, although the reduction was slightly smaller than that observed in fixed samples.

The lack of TIP47 interferes with the formation of mature LDs, probably at an early stage of their biogenesis, and might involve a change in cellular fatty acid uptake, neutral lipid synthesis, or liberation. Quantification of [^{14}C]-1-oleic acid uptake revealed that >100 fmol oleic acid/mg protein were internalized within 15 min into HeLa and TIP47 KD cells (Fig. 9 F).

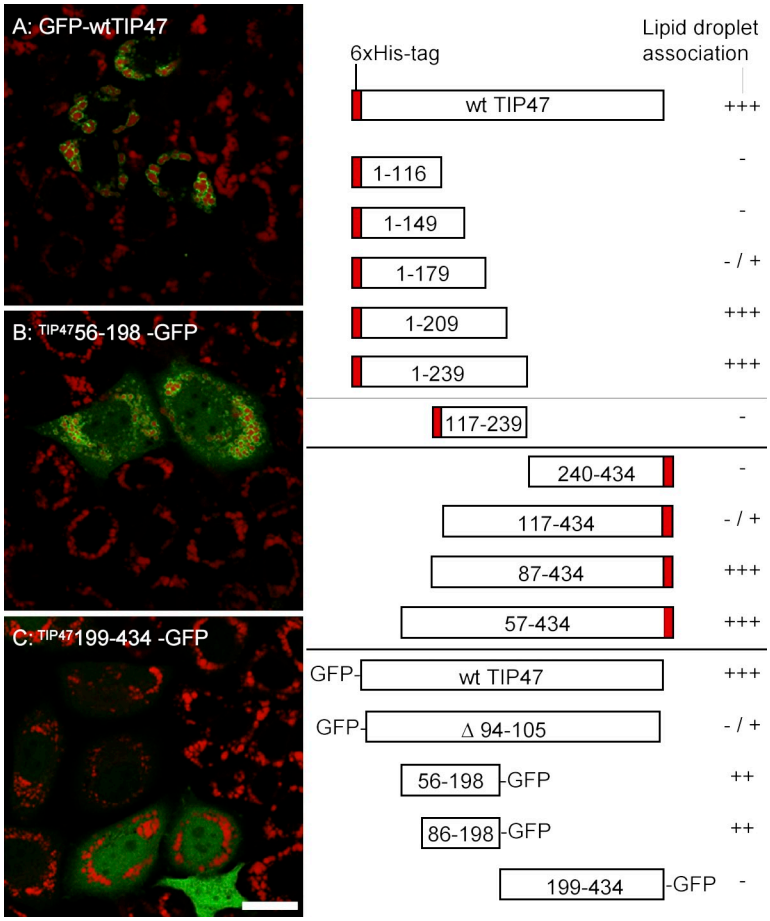

Figure 7. **The 11-mer repeat region of TIP47 is sufficient for LD targeting.** Variants of human TIP47 fused to a 6×His tag or to GFP were expressed in HeLa cells followed by analysis of LD recruitment after oleic acid feeding. The localization was classified as +++ if all protein was visible on the LD surface (A). ++ indicates LD labeling as well as cytoplasmic detection (B). −/+ indicates a dominant localization in the cytoplasm. − indicates lack of any LD staining (C). wt, wild type.

Furthermore, the amount and rate of palmitic and arachidonic acid uptake remained normal in RNAi cells (unpublished data), demonstrating that TIP47 is not involved in fatty acid uptake. Next, we analyzed the lipid composition of postnuclear supernatants (PNSs) and isolated LDs by TLC. The prominent lipid species in the PNSs were phosphatidylcholine, phosphatidylethanolamine, cholesterol, and TAG, whereas oleic acid and fatty acid esterified cholesterol were of low abundance. The quantification revealed that the TAG content of the PNS and of purified LDs of TIP47 KD cells was diminished by ∼30% (Fig. 9 H). Thus, KD of TIP47 interferes with TAG incorporation during normal LD maturation. Moreover, our subfractionation experiments may underestimate the reduction of TAG stored in LDs upon TIP47 KD if TAG accumulates in the ER of KD cells and ER-derived LD-like particles are generated during cell homogenization (see Discussion).

The suppression of TIP47 may also affect the release of fatty acids from intracellular lipid pools. However, ∼60% of the oleic acid initially stored as TAG was released by control and TIP47 KD cells within 6 h (unpublished data), suggesting that TIP47 is not an essential factor for lipolysis. In summary, we conclude that TIP47 is an important factor in the early phase of LD biogenesis that if missing affects the incorporation of TAG.

TIP47 has apolipoprotein-like properties in vitro

The function of TIP47 is unknown. To address this issue, we performed a functional analysis of recombinant TIP47 in vitro. First, we subjected TIP47 and GST as a control to Blue native gel electrophoresis to analyze oligomer formation. GST migrated in two bands compatible with the presence of 29-kD monomers and 58-kD dimers. TIP47 migrated in a single band below 140 kD, indicating the presence of dimers or trimers (Fig. 10 A). When cytosol was subjected to Blue native gel electrophoresis followed by detection of TIP47, the electrophoretic mobility of the cytosolic protein was identical to the recombinant counterpart (Fig. 10 B), and SDS-PAGE in the second dimension revealed that the Western blot signal belongs to a single protein with the expected molecular mass of TIP47 (Fig. 10 C). Although it is difficult to distinguish whether the electrophoretic mobility of TIP47 is consistent with dimers or trimers, analytical gel filtration through Superdex S200 (unpublished data) supports trimer formation.

For the last set of experiments, we were stimulated by the similarities between TIP47 and the exchangeable apolipoprotein apoE (Hickenbottom et al., 2004). Apolipoproteins play a key role in the formation and stability of lipoprotein particles that mediate the transport of neutral lipids through the circulation. ApoE is also a major determinant of lipoprotein particle recognition and uptake via the low density lipoprotein receptor and other related receptors (Hatters et al., 2006). The N-terminal domain of apoE and the C-terminal domain of TIP47 show high structural homology: both carry a bundle of four amphipathic α-helices. For apoE, it was shown that this four-helix bundle is reorganized upon interaction with lipids. Synthetic liposomes incubated with apoE in vitro undergo complete fragmentation

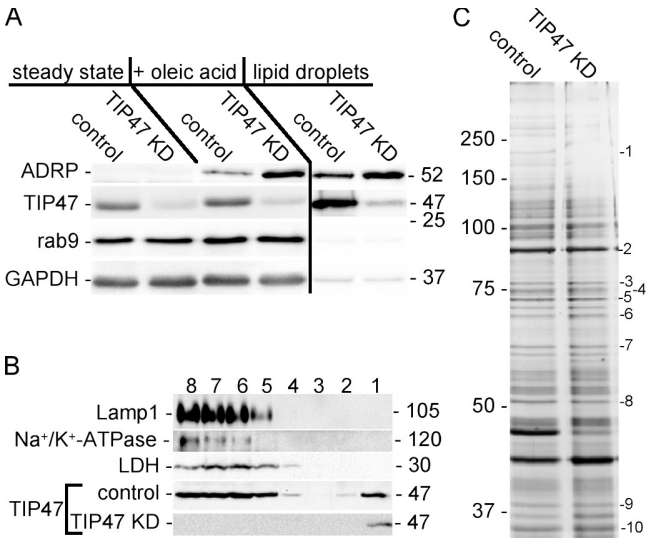

Figure 8. **TIP47 KD affects expression of ADRP.** (A) Western blot detection of the indicated proteins in cell lysates of control and TIP47 KD cells at steady state (lanes 1 and 2), after oleic acid feeding (lanes 3 and 4), and in isolated LDs (lanes 5 and 6). Black line indicates a seperate sample. (B) Detection of the indicated proteins in fractions derived from subcellular fractionation after oleic acid feeding. Lamp1, Na^+/K^+-ATPase, and lactate dehydrogenase served as marker proteins for late endosomes/lysosomes, the plasma membrane, and cytosol, respectively. TIP47 was detected in gradient fractions derived from control and TIP47 KD cells. (C) SDS-PAGE of LDs (equal amounts of protein) from HeLa and TIP47 KD cells. Proteins identified by peptide mass fingerprints included acetyl–coenzyme A carboxylase (1), Hsp90 (2), lanosterol synthase (3), BiP (4), Hsp70 (5), Hsp60 (6), ADRP (7 and 8), actin (9), and NAD phosphate–dependent steroid dehydrogenase (10). Values are shown in kilodaltons.

into small so-called disc structures. In these bilayer discs, which can be regarded as lipoprotein-like particles lacking their neutral lipid cargo, the acyl chains at the rim of the disc are shielded from the aqueous environment by the amphipathic helices of the apolipoprotein (Fig. 10 H; Raussens et al., 1998). Thus, disc formation is a measure of a protein's capacity to induce and/or stabilize a hydrophobic lipid assembly, a lipoprotein particle, or an LD.

We performed in vitro disc assays using DMPC liposomes incubated with TIP47 or GST and apoE as control proteins. After 16 h in absence (Fig. 10 D) or presence of protein, the samples were analyzed by EM (Fig. 10, E–G) or dynamic light scattering (not depicted). TIP47 fragmented liposomes into small discs with a diameter of 23 ± 4.1 nm, which is similar to those formed in the presence of apoE (Fig. 10, compare F with G), whereas liposomes incubated with GST remained intact (Fig. 10 E). When pure proteins were analyzed, no particulate material was visible, indicating that large protein aggregates were absent (unpublished data). In conclusion, recombinant TIP47 has apolipoprotein features and the potential to induce LD-like particles in vitro.

Discussion

Is TIP47 a sorting device for MPRs?

Delivery of lysosomal enzymes from the TGN to the endosomal system requires constant recycling of MPRs (Ghosh et al., 2003). Correct sorting of MPRs into vesicles destined for return to the TGN is thus an essential part of their itinerary. Although AP1, PACS1, retromer, and TIP47 are all implicated in cargo selection (Diaz and Pfeffer, 1998; Meyer et al., 2000; Arighi et al., 2004; Seaman, 2004; Scott et al., 2006), how MPR sorting factors/complexes are regulated in space and time is not understood.

TIP47 was discovered in a yeast two-hybrid screen as a binding protein of both MPR cytoplasmic tails and was the first protein described to mediate MPR retrograde sorting. Diaz and Pfeffer (1998) showed GTP-γS–driven recruitment of TIP47 to endosomal membranes in vitro and enhanced MPR300 degradation when TIP47 was depleted. Our data contradict these results. Neither MPR cytoplasmic tail showed TIP47 binding when probed with an SPR biosensor, whereas two known binding partners, the VHS domain of GGA1 and AP2, efficiently bound to the GST-MPR tail fusions. The TIP47 used in these assays is active in the context of lipid disc formation (see The function of TIP47 on LDs), arguing against nonfunctionality of the recombinant protein. MPR tail binding by TIP47 may also depend on secondary structure, which potentially is not preserved in our biosensor assay. However, cargo-binding adaptors whose structure was solved in the presence of a sorting signal (e.g., GGAs and APs) recognize sorting signals as largely nonstructured short linear sequences (Owen and Evans, 1998; Kato et al., 2002; Shiba et al., 2002; Kelly et al., 2008). GST fusions of MPR cytoplasmic tail fragments have also been used by others, although the experiments are distinct with respect to the readout of binding (Diaz and Pfeffer, 1998; Carroll et al., 2001). In the first publication on TIP47 as well as in subsequent studies that include images of TIP47 localization (Blot et al., 2003; Aivazian et al., 2006; Lopez-Verges et al., 2006), the staining is fuzzy and does not clearly label membranes that contain MPRs and/or Rab9, although the receptors and the GTPase are assumed to represent the main TIP47-binding partners. This is puzzling if one considers that the in vitro affinity of TIP47 binding to MPR was determined to K_d = 1–3 μM and even 300 nM in the presence of Rab9 (Krise et al., 2000; Carroll et al., 2001). We agree that TIP47 is localized to particulate structures at steady state in some cell types such as Cos-7, but those intracellular sites were unequivocally identified as LDs by double labeling with ADRP or a neutral lipid dye. If TIP47 is indeed important for MPR localization or lysosomal enzyme delivery, these processes should be dramatically affected in TIP47 KD cells. Such perturbations were not revealed by our analysis but are observed in cells lacking the retromer subunit Vps26 (Arighi et al., 2004; Seaman 2004; this study) or functional AP1 complexes (Meyer et al., 2000). Thus, our results argue against a function of TIP47 as a sorting device for MPRs.

TIP47 binding to Rab9

TIP47 was proposed to be a key effector of Rab9 (Aivazian et al., 2006). We were unable to detect localization of endogenous TIP47 on Rab9-positive structures or overlap between overexpressed YFP-TIP47 and CFP-Rab9 variants (wild type and constitutive active/inactive). We also failed to detect interaction between Rab9 and TIP47 by immunoprecipitation or by in vitro pull-down assays with recombinant proteins, analytical gel filtration, or in biosensor experiments. Others showed that TIP47 residues 161–169 (^{161}GVDKTK**SVV**TGG^{172}; human)

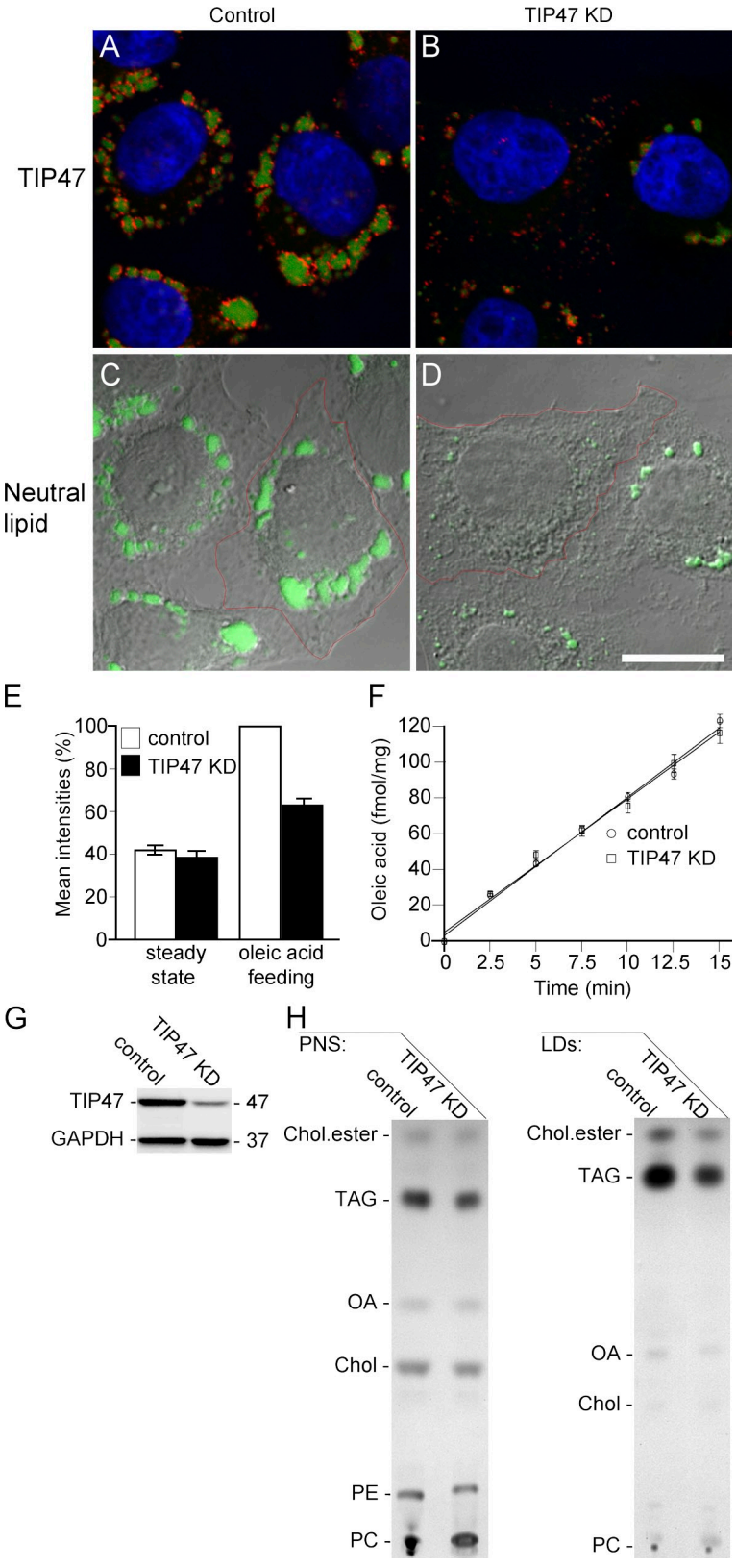

Figure 9. **Suppression of TIP47 affects LD maturation.** (A and B) TIP47 (red) and neutral lipid (green) after oleic acid feeding. (C and D) Merge of the differential interference contrast image and the neutral lipid stain of the cells shown in A and B. Fluorescence intensities were quantified per cell as indicated by the red regions. Bar, 15 µm. (E) Flow cytofluorometry of living cells. Bars in the first column represent the background geometric mean fluorescence intensities of Bodipy 493/503 in cells at steady state. Bars in the second column display the Bodipy 493/503 fluorescence intensities after oleic acid feeding. Error bars represent the variation of nine independent experiments. (F) Time course of [^{14}C]oleic acid uptake into cells. Error bars indicate the experimental variation between three experiments. (G) Verification of the TIP47 KD. Values on blot are shown in kilodaltons. (H) TLC of lipids from PNS and isolated LDs of control and TIP47 KD cells after oleic acid (OA) feeding. Chol, cholesterol; PE, phosphatidylethanolamine; PC, phosphatidylcholine.

are essential for Rab9 binding. Mutation of the three residues Ser-Val-Val (bolded in sequences) to triple Ala reduced Rab9 binding by 80%. Binding of the LD protein ADRP, which is the closest relative of TIP47 and contains the sequence ^{148}SVEKTK**SVV**SGS^{159}, was negligible (Hanna et al., 2002). The authors speculate that subtle conformational differences may cause the dramatic differences in Rab9 binding of TIP47 compared with ADRP. If so, how Rab9 binding to TIP47 occurs in mice is unclear, as the respective mouse TIP47 sequence (^{165}SVDKTK**SAM**TSG^{176}) is even less homologous to human ADRP.

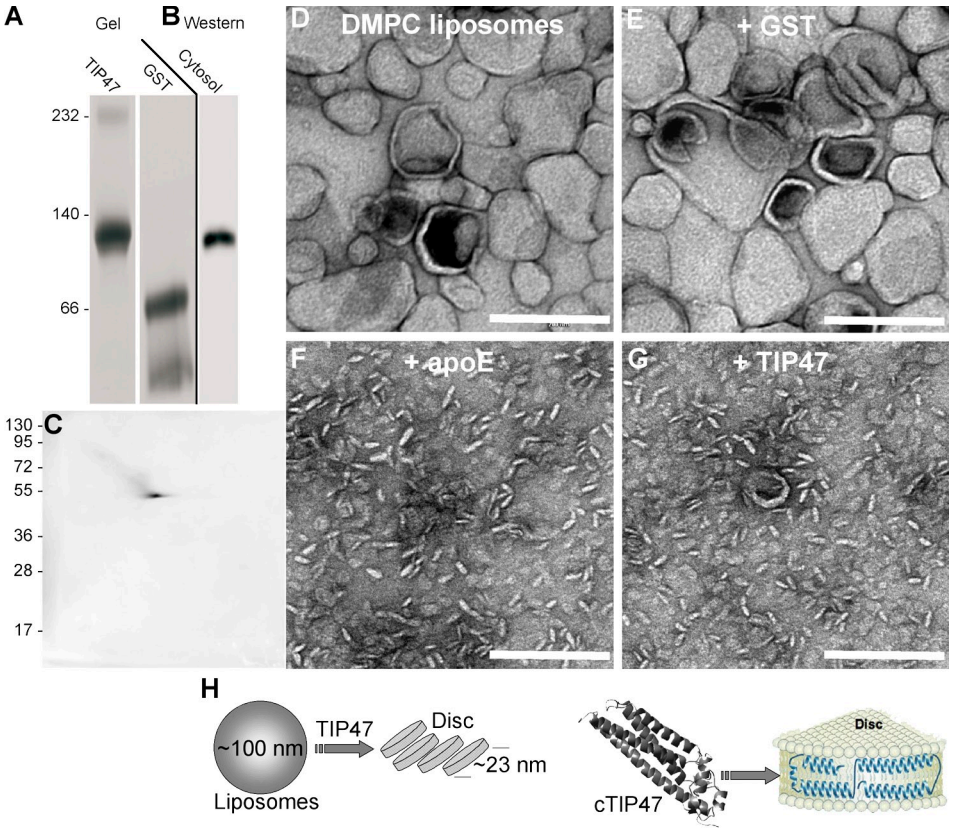

Figure 10. **Recombinant TIP47 has apolipoprotein-like properties.** (A) Blue native electrophoresis of recombinant TIP47 and GST. Black line indicates a seperate sample. (B) Detection of TIP47 in a Western blot after blue native electrophoresis of HeLa cytosol. (C) Western blot detection of TIP47 after 2D blue native electrophoresis/SDS-PAGE. (D–G) Analysis of a lipid disc assay by EM after DMPC liposomes (~100 nm diameter) had been incubated for 12 h with buffer (D) in presence of GST (E), apoE (F), or TIP47 (G). (H) Cartoon adapted from Raussens et al. (1998), illustrating the fragmentation of bilayered liposomes into lipid discs (not drawn to scale). Disc formation is thought to involve the refolding of the compact C-terminal domain of TIP47 into separate helices that shield the lipid acyl chains from the aqueous buffer environment. Values on gel blots are shown in kilodaltons. Bars, 200 nm.

Typically, extensive structural changes in the GTPase switch regions upon nucleotide exchange allow effectors to strongly discriminate between the GDP- or GTP-bound versions of a Rab protein. For example, binding of EEA1 to GDP-bound Rab5c is undetectable, whereas binding to Rab5c loaded with GppNHp has a K_d of 2.3 μM (Merithew et al., 2003). Likewise, the Rab11 effector sec15 binds GTP-Rab11 with 10-fold higher affinity than GDP-Rab11 (Zhang et al., 2004). However, as the reported affinity of TIP47 for GTP–Rab9 (96 nM) is only twofold higher than for GDP-Rab9 (159 nM; Carroll et al., 2001; Ganley et al., 2004), it is questionable whether TIP47 can be regarded as a typical Rab effector.

Cells lacking ~80–90% of TIP47 showed no change in Rab9 expression or the cytosol to membrane ratio of Rab9, which is in contrast to previous studies (Ganley et al., 2004; Aivazian et al., 2006). Use of different RNAi sequences may account for this inconsistency; however, we used the published TIP47 and Rab9 siRNA target sequences as well as additional ones. In fact, none of the five target sequences used to deprive cells of TIP47 affected expression of Vps35, Vps26, GAPDH (glyceraldehyde 3-phosphate dehydrogenase), AP2 α-subunit, AP1 γ-subunit, or actin. However, we consistently observed two- to fourfold higher expression of ADRP, the closest TIP47 relative, in TIP47 KD cells. It is thus unlikely that the discrepant results are caused by use of different TIP47 RNAi target sequences. RNAi efficiency is always an issue, but suppression of TIP47 expression is evident in our experiments both by Western blot analysis and immunoprecipitation from metabolically labeled cells. Moreover, TIP47 KD cells do have a phenotype, although it is manifested as perturbed formation of LDs and neutral lipid incorporation, not as disruption of Rab9 or MPR functionality.

The recruitment of TIP47 to LDs

A key finding of this work is that TIP47 is recruited to nascent LDs within minutes after oleic acid administration. The localization of TIP47 to LDs was doubted (Barbero et al., 2001), but we believe that the data presented in this study clearly demonstrate that TIP47 is associated with and functions on LDs. This notion is supported by data from other groups that showed LD localization of TIP47 by immunofluorescence (Wolins et al., 2001; Than et al. 2003; Orlicky et al., 2008) and EM using immunogold labeling techniques (Robenek et al., 2005). In addition, an unbiased proteomics approach identified TIP47 as a protein component of LDs (Brasaemle et al., 2004). In our isolated LDs, TIP47 was more abundant than ADRP, but this should be interpreted with caution because we know little about the binding (direct or indirect) of associated proteins to the LD surface and their susceptibility to the washing conditions during

the purification procedure. In extracts of TIP47 KD cells, we consistently detected a two- to fourfold higher expression of ADRP, indicating that the cells try to compensate the TIP47 deficiency. It may also indicate that LD targeting of ADRP can occur independent of TIP47. Similar to Liu et al. (2004), we found several members of the Rab family of proteins (Rab1, Rab5, Rab7, and Rab11) associated with LDs. It is tempting to speculate that LDs are linked to trafficking pathways such that they provide a source for membrane lipids or function as a temporary docking site for factors that only transiently attach to membranes like the Rabs, but the relevance of this speculation has to await its experimental verification.

We showed that the N-terminal half of TIP47 harbors the critical sequence elements (residues 87–198) for targeting to the LD surface. This finding is in contrast to a recent study that proposed targeting via the C-terminal hydrophobic cleft-containing part (Ohsaki et al., 2006). However, surprisingly, these authors also found that neither a tagged wild-type TIP47 nor the C-terminal half of TIP47 on its own showed LD localization despite the presence of the putative targeting sequence. In this study, we observed a clearcut sequence requirement for TIP47 targeting. The C-terminal fragment did not localize to the LD surface but was found cytosolic (Fig. 7). This suggests that the N-terminal half of TIP47 contains the necessary sequence information for LD targeting. Indeed, residues 87–198 were sufficient for recruitment of GFP. This fits well with recent data on ADRP, identifying the sequence stretch 89–202 for LD recruitment (McManaman et al., 2003; Orlicky et al., 2008). The sequence 87–198 of TIP47 contains 11-mer repeats that are thought to form amphipathic helices, which raises the attractive possibility that these helices mediate the initial attachment of TIP47 and ADRP to the LD surface.

The function of TIP47 on LDs

KD of TIP47 results in defects in the cellular response to feeding with oleic acid. Although the uptake of fatty acids, the breakdown of TAG, and the export of fatty acids from the cells remain normal, the growth and maturation of LDs are inhibited. In immunofluorescence, the droplets appeared heterogeneous with respect to size, and the amount of LD-stored TAG was reduced even though we were unable to suppress TIP47 completely. The reduction in LD-stored TAG was confirmed by lipid analysis of isolated LDs. We consider it unlikely that TIP47 has a direct function in neutral lipid synthesis. Instead, KD of TIP47 probably affects the cellular capacity to store neutral lipids in LDs. If so, TAG or precursors such as diacylglycerol should accumulate elsewhere in the cell, for example, at or between dilated ER leaflets. Unfortunately, it is very difficult to validate this hypothesis because such structures are probably smaller than the spatial resolution of light microscopy and very fragile, thus escaping detection in fractionation experiments. During cell homogenization, ER sites of neutral lipid accumulation may fragment into LD-like particles that contaminate the LD fraction. Clearly, novel methods and assays are required to address the biogenesis and maturation of LDs.

One approach to tackle the function of a protein is to reconstitute its functional properties in vitro under defined conditions. In this study, we demonstrated for the first time that TIP47 as a member of the PAT protein family has lipid-organizing properties equivalent to those of well-known exchangeable apolipoproteins. TIP47 fragments DMPC liposomes into small 23-nm lipid discs. Such discs can only be formed if the acyl chains at the rim of the disc are shielded from the aqueous environment by amphipathic helices. Thus, lipid disc formation is accompanied by a complete structural rearrangement of TIP47, probably involving unfolding of the C-terminal amphipathic helix bundle. This notion is confirmed by cryo-EM analysis of disc formation in the presence of the recombinant C-terminal TIP47 fragment alone (unpublished data). Although the C-terminal domain of TIP47 can induce lipid disc formation in vitro, it fails to mediate LD recruitment in cells (Fig. 7). This suggests that the N- and C-terminal domains of TIP47 carry out separate functions in LD targeting and in stabilization of the growing LD surface, respectively. The same is observed for apoE: the N-terminal domain containing the amphipathic helix bundle induces lipid discs in vitro, whereas the C-terminal domain is primarily responsible for binding to lipoprotein particles in vivo. Taking into account that cytosolic TIP47 exists as trimers or even higher oligomeric forms, the role of oligomerization in the function of TIP47 remains to be elucidated.

TIP47 relocalizes to sites of LD formation within minutes after oleic acid feeding of cells, but how? Assuming that LDs originate from the ER, an associated protein factor may be required for recruitment of TIP47. Alternatively, neutral lipid synthesis within the ER membrane may cause an increase in phospholipid headgroup spacing, which is sensed by TIP47 via its N-terminal 11-mer repeat amphipathic helices. After initial binding, the C-terminal four-helix bundle may unfold to further cover the hydrophobic defects that arise during rapid intramembrane accumulation of neutral lipid and allow LD growth. In addition to this and in analogy to apolipoproteins, the open form of the TIP47 C-terminal helices may also be a platform for interactions with yet unknown binding partners. Finally, there is no conclusive experimental proof for neutral lipid accumulation within the ER membrane, and thus, it cannot be excluded that PAT proteins such as TIP47 function in the formation of small ER-derived lipid discs into which newly synthesized neutral lipid as well as further phospholipids are incorporated.

Materials and methods

Antibodies

For detection of TIP47, we used guinea pig antibodies (Progen), an affinity-purified rabbit serum (provided by S. Pfeffer, Stanford University, Palo Alto, CA), a rabbit serum (provided by G. Than, University of Pécs, Pécs, Hungary), or rabbit sera generated by us (Fig. S3). Anti-ADRP was obtained from Progen, anti-Lamp1 and anti-Na^+/K^+-ATPase from the Hybridoma Bank, anti-transferrin receptor from Invitrogen, antibodies for EEA1, α-catenin, α-adaptin and GM130 from Transduction, anti-Rab9 from Enzo Biochem, Inc. or Thermo Fisher Scientific, anti-TGN46 from AbD Serotec, anti-GAPDH from Millipore, anti-VPS26 and anti-VPS35 from M. Seaman (Cambridge Institute for Medical Research, Cambridge, England, UK), monoclonal anti-His antibody from QIAGEN, and monoclonal anti-HA from Babco. Alexa Fluor 546–conjugated human transferrin and all fluorochrome-conjugated secondary antibodies were obtained from Invitrogen, and secondary antibodies for Western blotting were obtained from Dianova. The antibodies against MPR46 (10C6, monoclonal), MPR300 (VII-2, rabbit), CatD (rabbit), and TIP47 (rabbit) were generated in our department.

Reagents

Neutral lipid was stained with reagents from Invitrogen: 0.1 µg/ml Nile red, 500 nM Bodipy 493/503, high content screening LipidTox red (1:1,000), or high content screening LipidTox deep red (1:1,000).

Cell culture and transfection
Cells were grown in DME, 10% FCS at 37°C, and 5% CO_2. HeLa cells stably expressing TIP47 hairpin RNA were selected in medium containing 500 µg/ml G418. For some experiments, cells were starved by overnight incubation with medium containing 2% serum. Fatty acids used for feeding experiments were complexed with fat-free BSA (Sigma-Aldrich) at a molar ratio of 6:1. Oleic acid was used at a final concentration of 400 µM. DNA was transfected into HeLa cells using Effectene (QIAGEN) according to the manufacturer's instructions.

Cloning of recombinant TIP47 and Rab9
The full-length cDNA of human TIP47 was cloned by RT-PCR from total HeLa cell RNA into the mammalian expression vector pMPSV-EH. This cDNA served as a template for the generation of TIP47 containing an HA tag or a His tag at either the N or C terminus. To generate EGFP-TIP47 chimera, the human TIP47 cDNA was amplified by PCR and subsequently cloned into pTagRFP-C, pTagGFP-C, pTagCFP (Evrogen), and pEYFP-C1 (Clontech Laboratories, Inc.). Truncated TIP47 variants were engineered with primers that introduced artificial start and/or stop codons. For bacterial expression of recombinant TIP47, the cDNA of TIP47 was cloned into the pETM30 expression vector.

Canine Rab9 cDNA was amplified by PCR from pET3d-Rab9 (provided by S. Pfeffer) using XhoI and BamHI cloning sites. The obtained cDNA encoded for a protein with an altered C-terminal sequence: Ser-Cys-Lys-Lys-Lys-COOH. This sequence was corrected for the original sequence of the protein: Ser-Cys-Cys-COOH to allow prenylation of both cysteins. The cDNA was subsequently cloned in frame into pTag variants. The mutant forms of Rab9, Rab9 S21N (dominant negative), and Rab9 Q66L (constitutively active) were generated with the QuickChange site-directed mutagenesis kit (Agilent Technologies).

The exact sequences of all primers as well as all cDNAs are available upon request. The identity of the Rab9 cDNA, TIP47 cDNA, and all derived variants was confirmed by sequencing of the complete coding sequence.

RNAi
For transient RNAi, we used siRNA oligonucleotides from Applied Biosystems. Two different oligonucleotides (30 nM each) were transfected for 2 d in a row using Lipofectamine 2000 (Invitrogen) according to the manufacturer's protocol. Cells were analyzed 72 h after the first siRNA transfection. In the case of oleic acid treatment, cells were fed with oleic acid 72 h after the first transfection and investigated thereafter. We also established a plasmid-based system to stably suppress the expression of TIP47 in HeLa cells, using the sequence 5′-CCCGGGGCTCATTTCAAAC-3′ starting at position 1,435 in the 3′ untranslated region of human TIP47 mRNA as a target.

Flow cytofluorometry
16 h after lipid feeding, the cells were incubated in the presence of Bodipy 493/503 for 2 h followed by washing and separation of the cells with trypsin. After centrifugation and washing, the cells were resuspended in 1 ml ice-cold PBS. A minimum of 30,000 cells were analyzed using an FACS flow cytometer (Canto; BD) equipped with Diva software (BD). Measurements of forward scatter were used to exclude dead cells and debris.

Immunofluorescence
The procedure follows a recently published protocol (Chapuy et al., 2008) using either paraformaldehyde (20 min at 25°C) or methanol (−20°C for 5 min) for fixation. The cells were routinely permeabilized with 0.5% saponin in PBS and, in some experiments, it was substituted for 0.1% Triton X-100. For the detection of LDs and the cellular DNA, the neutral lipid dye and DAPI were added to the secondary antibody solution. All images shown in this study represent confocal sections obtained with a 60× Plan Apo NA 1.42 lens of a confocal laser-scanning microscope (IX81; Olympus). The FluoView software (FV1000; Olympus) was used to control the microscope settings and for quantification of fluorescence intensities. All images were put together using Photoshop software (Adobe) but without any further manipulation of contrast or brightness. For quantification, confocal sections were taken 1 µm from the coverslip surface. The differential interference contrast images served as a template to mark the area of all individual cells of the section followed by determination of the intensity per micrometer-squared cell area of ∼100 cells.

Lipid disc formation, dynamic light scattering, and EM
100 nm liposomes (DMPC) were prepared as described previously (Höning et al., 2005) and incubated overnight at 25°C with/without TIP47, apoE, or GST at a ratio of 1:3.75 (wt/wt; 50 µl total volume). Subsequently, an aliquot of the mixture was applied to carbon-coated/glow-discharged grids (400 mesh) for 5 min then fixed with 0.1% glutaraldehyde and negatively stained with 1% uranyl acetate. EM micrographs were taken at a magnification of 56,000× and used for size determination of the lipid discs (n = 100–300) with the iTEM program of the transmission EM imaging platform (Olympus). The mean diameter was 23 ± 4.1 nm. Similar values were obtained by dynamic light scattering in a Protein Solutions instrument (DynaPro). 20 µl of all lipid/protein samples were analyzed with an acquisition time of 10 s and a total of 30 acquisitions. Changes in the hydrodynamic radius of the liposomes were evaluated with the software supplied by the manufacturer (Dynamics V6).

Fatty acid uptake experiments
HeLa and TIP47 RNAi cells seeded at equal densities in 3-cm dishes were grown for 24 h, washed, and incubated in fresh medium containing a trace of [1-^{14}C]–labeled oleic acid (330 nCi/ml, specific activity 53 mCi/mmol) supplemented with nonlabeled oleic acid/BSA to a final concentration of 600 µM. Uptake of palmitic acid and arachidonic acid was determined in the same way but at final concentrations of 20 µM and using [9,10-^{3}H]palmitic acid and [1-^{14}C]arachidonic acid as radiolabeled tracers. After addition of the fatty acid feeding medium, the cells were incubated for periods up to 2 h, washed, harvested, homogenized, and used for counting of TCA-precipitable radioactivity and determination of the protein concentration. All experiments were performed as triplicates and repeated twice. All values shown were normalized for the amount of protein.

Release of fatty acids from stored neutral lipid
To quantify the release of free fatty acids from stored lipid pools, two dishes of HeLa and RNAi cells were incubated in medium supplemented with [1-^{14}C]oleic acid (as described in Fatty acid uptake experiments). Subsequently, the cells were placed on ice and washed with PBS containing 1% fatty acid free BSA followed by collecting cells of dish 1 to determine the amount of protein and quantification of radioactivity. To assay the efflux of fatty acid from the labeled cells, the remaining dish was incubated up to 6 h in DME without FCS but supplemented with 1% fatty acid free BSA as a fatty acid acceptor. 10 µM triacsin C, a known inhibitor of the fatty acid acyl coenzyme A ligase, was added to block reesterification of released fatty acids (Tansey et al., 2003). After the indicated times, an aliquot of the efflux medium was used for quantification of the radioactivity. The cellular lipid was analyzed by TLC (as described in Lipid extraction and TLC). TLC revealed that the radioactivity in the medium was essentially free oleic acid.

Sorting of lysosomal enzymes
The enzymatic activity of β-hexosaminidase was determined as previously described in Chapuy et al., (2008). The amount of CatD in cells and media was determined by Western blots as described previously (Perez-Victoria et al., 2008).

LD isolation
After overnight incubation with 400 µM oleic acid in DME + 10% FCS, the cells from a single 15-cm dish were collected in ice-cold PBS, washed once, and centrifuged at 500 g for 5 min. The cell pellet was resuspended in 1 ml buffer A (20 mM Tris, pH 7.8, and 250 mM sucrose), homogenized by 10 passages through a 27-gauge needle, and centrifuged at 500 g for 5 min to receive a PNS. 2.5 mg protein of the PNS was adjusted to 7 ml of buffer A overlayed with 3.5 ml buffer B (20 mM Hepes, pH 7.4, 100 mM KCl, and 2 mM $MgCl_2$) followed by centrifugation at 200,000 g (SW41 rotor; Beckman Coulter) for 4 h. Subsequently, the tube was placed in a tube slicer (Beckman Coulter) and cut 0.75 cm from the top of the gradient. The upper LD fraction (∼1 ml) was transferred into a glass vial, and the tube was washed four times with methanol to collect all LDs for lipid extraction.

Lipid extraction and TLC
Lipid extraction was performed as described in Wessel and Flugge (1984). The resulting lipid phase was transferred into a new glass vial and evaporated under nitrogen. The dried lipids were stored at −20°C until further use. The TLC plates (silica 60 W F254; 20 × 20 cm; Merck) were prerun in methanol, dried, and activated for 10 min at 110°C on a TLC plate heater (TLC plate heater III; CAMAG). Standards and samples were applied with capillaries followed by development of the plate in solvent 1 (acid methylester, 1-propanol, chloroform, methanol, and 0.25% KCl [ratio 3:3:3:2:1]) to 4 cm. The plate was removed from the tank and dried. Solvent 2 (75% N-hexan, 23% diethyl ether, and 2% acetic acid) and solvent 3 (N-hexan) were allowed to migrate to 1 cm from the top of the plate. For lipid detection, the plates were dipped in

10% phosphoric acid and 7.5% copper-sulfate and developed at 170°C on a TLC plate heater. Quantification was performed with a Reprostar 3 (CAMAG).

Purification of recombinant TIP47 and Rab9; GTPase and interaction assays

The cDNAs for TIP47 and Rab9 were cloned into pET-M30, a modified pET vector coding for a tobacco etch virus protease recognition site between an N-terminal His_6-GST tag and the protein of interest. Both proteins were purified using GSH-Sepharose affinity chromatography followed by cleavage of the fusion protein with tobacco etch virus protease, Ni^{2+}-NTA affinity chromatography, and gel filtration chromatography on a Sephadex column (26/60; S200; GE Healthcare) to prove monodispersity and remove aggregates. The purified Rab9 is bound exclusively to GDP as found by HPLC (Tucker et al., 1986). Nucleotide exchange on Rab9 for GTP and the nonhydrolysable GTP analogue GppNHp was performed essentially as described (John et al., 1988). The intrinsic Rab9 GTPase activity was determined at 25°C by following the single exponential decrease of the GTP content in the Rab9–GTP complex via HPLC. To test for nucleotide-dependent binding of TIP47 and Rab9, pull-down assays using Talon beads (Clontech Laboratories, Inc.) were performed at 25°C. The affinity matrix was loaded with His_6-GST-TIP47 and equilibrated in 20 mM Tris/HCl, pH 8.0, 100 mM NaCl, 2 mM 2-mercaptoethanol, and 5 mM $MgCl_2$ (binding buffer). An equimolar amount of Rab9 complexed with GDP, GTP, or GppNHp was added and incubated for 2 h. After washing with 10-column volumes of binding buffer containing 15 mM imidazole, bound proteins were eluted with binding buffer containing 500 mM imidazole and analyzed by SDS-PAGE. Analytical gel filtration was performed on a column (10/30; S75; GE Healthcare) in 20 mM Hepes/NaOH, pH 7.4, and 5 mM $MgCl_2$ using TIP47 and Rab9 complexed with GppNHp or GTP both individually and as an equimolar mixture that was incubated for 2 h before loading onto the column. Peak fractions were analyzed by SDS-PAGE.

SPR biosensor experiments

The interaction between the tails of MPR 46, MPR300, and TIP47 was analyzed in vitro using an SPR biosensor (Biacore 3000; Biacore). The complete cytoplasmic tail of human MPR46 was fused in frame to the C terminus of GST, expressed in *Escherichia coli* BL21, and purified from the bacteria to homogeneity. The GST fusion of the MPR300 cytoplasmic tail was provided by T. Braulke (University of Hamburg, Hamburg, Germany). Both GST-MPR tail fusions and GST as a control were coupled to a CM5 sensor surface using amino coupling. After immobilization, the binding of soluble TIP47, GST, GST-VHS, and AP2 was recorded at a flow rate of 30 µl/min. All proteins were injected at concentrations ranging from 200 nM to 25 µM. Association was recorded for 1 min followed by a dissociation period of 2 min. After this period, the surface was regenerated with a 5-s pulse injection of 50 mM NaOH. All binding experiments were performed in three different buffers, A (10 mM Tris, pH 7.5, 250 mM NaCl, and 5 mM DTT), B (25 mM Hepes, pH 7.2, 150 mM NaCl, 0,1% Triton X-100, and 5 mM DTT), and C (PBS, pH 7.4, and 5 mM DTT).

Identification of proteins by mass spectrometry

For peptide mass fingerprint analysis, the respective protein bands visible after Coomassie staining were excised, cut into small 1-mm pieces, subjected to in-gel digestion with trypsin (Shevchenko et al., 2002), desalted on C18 ZipTIP, and analyzed by matrix-assisted laser desorption/ionization time of flight mass spectrometry using dihydrobenzoic acid as matrix and two autolytic peptides of trypsin (m/z 842.51 and 2211.10) as internal standards. The mass spectrometric data were used by Mascot search algorithm for protein identification in the NCBInr protein database.

Western blotting

Samples were resolved by SDS-PAGE under denaturing conditions using small slab gels (Bio-Rad Laboratories). For Western blots, proteins were transferred onto 0.2 µm nitrocellulose (Schleicher & Schuel) followed by blocking in 5% dry milk in PBS and 0.05% Tween. The incubation with the first antibodies was performed for 1 h at room temperature followed by washing and incubation for 1 h with the respective secondary antibodies (Dianova). Signals were detected using a charge-coupled device camera (Fluor Chem SP; Alpha Innotech).

Blue native electrophoresis

HeLa cell cytosol or recombinant TIP47 was resuspended in lysis buffer (20 mM Bis-Tris, 500 mM ε-aminocaproic acid, 20 mM NaCl, 2 mM EDTA, and 10% glycerol, pH 7.0) containing 0.5% digitonin. The lysates were separated by 10–20% gradient blue native gels at 4°C as described previously (Schägger et al., 1994). A high molecular weight calibration kit (GE Healthcare) for native electrophoresis was used as a standard for molecular weight determination. For 2D analysis, proteins were first resolved by blue native electrophoresis, and the protein-containing lanes were cut (Swamy et al., 2006) and resolved by conventional SDS-PAGE.

Online supplemental material

Fig. S1 shows that TIP47 does not colocalize with MPR46 but with ADRP to the surface of LDs in four different human cell lines. Fig. S2 shows that TIP47 is not detectable on membranes of the biosynthetic and endocytic pathways in HeLa cells. Fig. S3 shows that all antibodies against TIP47 that were available to us detect a single protein in immunoprecipitations and Western blots with a molecular mass that matches that of TIP47. Fig. S4 shows that YFP-TIP47 is recruited to LDs as indicated by colabeling with endogenous ADRP but not to membranes that contain MPR46. Fig. S5 shows the time course of TIP47 recruitment to LDs after administration of oleic acid. Online supplemental material is available at http://www.jcb.org/cgi/content/full/jcb.200812042/DC1.

We thank Andrea Rüger and Ireen Schaffrath for expert technical assistance and members of the Höning laboratory for valuable suggestions. We gratefully acknowledge Suzanne Pfeffer, Gabor Than, and Matthew Seaman for their generous gifts of antibodies.

This work was supported by the Cologne Center for Molecular Medicine (TP C3) and the Deutsche Forschungsgemeinschaft (SFB 635, TP A3).

Submitted: 11 December 2008
Accepted: 21 April 2009

References

Aivazian, D., R.L. Serrano, and S. Pfeffer. 2006. TIP47 is a key effector for Rab9 localization. *J. Cell Biol.* 173:917–926.

Arighi, C.N., L.M. Hartnell, R.C. Aguilar, C.R. Haft, and J.S. Bonifacino. 2004. Role of the mammalian retromer in sorting of the cation-independent mannose 6-phosphate receptor. *J. Cell Biol.* 165:123–133.

Barbero, P., E. Buell, S. Zulley, and S.R. Pfeffer. 2001. TIP47 is not a component of lipid droplets. *J. Biol. Chem.* 276:24348–24351.

Blot, G., K. Janvier, S. Le Panse, R. Benarous, and C. Berlioz-Torrent. 2003. Targeting of the human immunodeficiency virus type 1 envelope to the trans-Golgi network through binding to TIP47 is required for env incorporation into virions and infectivity. *J. Virol.* 77:6931–6945.

Bonifacino, J.S., and R. Rojas. 2006. Retrograde transport from endosomes to the trans-Golgi network. *Nat. Rev. Mol. Cell Biol.* 7:568–579.

Brasaemle, D.L. 2007. Thematic review series: adipocyte biology. The perilipin family of structural lipid droplet proteins: stabilization of lipid droplets and control of lipolysis. *J. Lipid Res.* 48:2547–2559.

Brasaemle, D.L., G. Dolios, L. Shapiro, and R. Wang. 2004. Proteomic analysis of proteins associated with lipid droplets of basal and lipolytically stimulated 3T3-L1 adipocytes. *J. Biol. Chem.* 279:46835–46842.

Bussell, R., Jr., and D. Eliezer. 2003. A structural and functional role for 11-mer repeats in alpha-synuclein and other exchangeable lipid binding proteins. *J. Mol. Biol.* 329:763–778.

Carroll, K.S., J. Hanna, I. Simon, J. Krise, P. Barbero, and S.R. Pfeffer. 2001. Role of Rab9 GTPase in facilitating receptor recruitment by TIP47. *Science.* 292:1373–1376.

Chapuy, B., R. Tikkanen, C. Muhlhausen, D. Wenzel, K. von Figura, and S. Honing. 2008. AP-1 and AP-3 mediate sorting of melanosomal and lysosomal membrane proteins into distinct post-Golgi trafficking pathways. *Traffic.* 9:1157–1172.

Diaz, E., and S.R. Pfeffer. 1998. TIP47: a cargo selection device for mannose 6-phosphate receptor trafficking. *Cell.* 93:433–443.

Falcon-Perez, J.M., R. Nazarian, C. Sabatti, and E.C. Dell'Angelica. 2005. Distribution and dynamics of Lamp1-containing endocytic organelles in fibroblasts deficient in BLOC-3. *J. Cell Sci.* 118:5243–5255.

Ganley, I.G., K. Carroll, L. Bittova, and S. Pfeffer. 2004. Rab9 GTPase regulates late endosome size and requires effector interaction for its stability. *Mol. Biol. Cell.* 15:5420–5430.

Ghosh, P., N.M. Dahms, and S. Kornfeld. 2003. Mannose 6-phosphate receptors: new twists in the tale. *Nat. Rev. Mol. Cell Biol.* 4:202–212.

Hanna, J., K. Carroll, and S.R. Pfeffer. 2002. Identification of residues in TIP47 essential for Rab9 binding. *Proc. Natl. Acad. Sci. USA.* 99:7450–7454.

Hatters, D.M., C.A. Peters-Libeu, and K.H. Weisgraber. 2006. Apolipoprotein E structure: insights into function. *Trends Biochem. Sci.* 31:445–454.

Hickenbottom, S.J., A.R. Kimmel, C. Londos, and J.H. Hurley. 2004. Structure of a lipid droplet protein; the PAT family member TIP47. *Structure.* 12:1199–1207.

Höning, S., D. Ricotta, M. Krauss, K. Späte, B. Spolaore, A. Motley, M. Robinson, C. Robinson, V. Haucke, and D.J. Owen. 2005. Phosphatidylinositol-(4,5)-bisphosphate regulates sorting signal recognition by the clathrin-associated adaptor complex AP2. *Mol. Cell.* 18:519–531.

John, J., M. Frech, and A. Wittinghofer. 1988. Biochemical properties of Ha-ras encoded p21 mutants and mechanism of the autophosphorylation reaction. *J. Biol. Chem.* 263:11792–11799.

Kato, Y., S. Misra, R. Puertollano, J.H. Hurley, and J.S. Bonifacino. 2002. Phosphoregulation of sorting signal-VHS domain interactions by a direct electrostatic mechanism. *Nat. Struct. Biol.* 9:532–536.

Kelly, B.T., A.J. McCoy, K. Spate, S.E. Miller, P.R. Evans, S. Honing, and D.J. Owen. 2008. A structural explanation for the binding of endocytic dileucine motifs by the AP2 complex. *Nature.* 456:976–979.

Krise, J.P., P.M. Sincock, J.G. Orsel, and S.R. Pfeffer. 2000. Quantitative analysis of TIP47-receptor cytoplasmic domain interactions: implications for endosome-to-trans Golgi network trafficking. *J. Biol. Chem.* 275:25188–25193.

Kuerschner, L., C. Moessinger, and C. Thiele. 2008. Imaging of lipid biosynthesis: how a neutral lipid enters lipid droplets. *Traffic.* 9:338–352.

Liu, P., Y. Ying, Y. Zhao, D.I. Mundy, M. Zhu, and R.G.W. Anderson. 2004. Chinese hamster ovary K2 cell lipid droplets appear to be metabolic organelles involved in membrane traffic. *J. Biol. Chem.* 279:3787–3792.

Lopez-Verges, S., G. Camus, G. Blot, R. Beauvoir, R. Benarous, and C. Berlioz-Torrent. 2006. Tail-interacting protein TIP47 is a connector between Gag and Env and is required for Env incorporation into HIV-1 virions. *Proc. Natl. Acad. Sci. USA.* 103:14947–14952.

McManaman, J.L., W. Zabaronick, J. Schaack, and D.J. Orlicky. 2003. Lipid droplet targeting domains of adipophilin. *J. Lipid Res.* 44:668–673.

Merithew, E., C. Stone, S. Eathiraj, and D.G. Lambright. 2003. Determinants of Rab5 interaction with the N terminus of early endosome antigen 1. *J. Biol. Chem.* 278:8494–8500.

Meyer, C., D. Zizioli, S. Lausmann, E.-L. Eskelinen, J. Hamann, P. Saftig, K. von Figura, and P. Schu. 2000. {micro}1A-adaptin-deficient mice: lethality, loss of AP-1 binding and rerouting of mannose 6-phosphate receptors. *EMBO J.* 19:2193–2203.

Miura, S., J.-W. Gan, J. Brzostowski, M.J. Parisi, C.J. Schultz, C. Londos, B. Oliver, and A.R. Kimmel. 2002. Functional conservation for lipid storage droplet association among Perilipin, ADRP, and TIP47 (PAT)-related proteins in mammals, *Drosophila*, and *Dictyostelium*. *J. Biol. Chem.* 277:32253–32257.

Ohsaki, Y., T. Maeda, M. Maeda, K. Tauchi-Sato, and T. Fujimoto. 2006. Recruitment of TIP47 to lipid droplets is controlled by the putative hydrophobic cleft. *Biochem. Biophys. Res. Commun.* 347:279–287.

Orlicky, D.J., G. Degala, C. Greenwood, E.S. Bales, T.D. Russell, and J.L. McManaman. 2008. Multiple functions encoded by the N-terminal PAT domain of adipophilin. *J. Cell Sci.* 121:2921–2929.

Owen, D.J., and P.R. Evans. 1998. A structural explanation for the recognition of tyrosine-based endocytotic signals. *Science.* 282:1327–1332.

Perez-Victoria, F.J., G.A. Mardones, and J.S. Bonifacino. 2008. Requirement of the human GARP Complex for mannose 6-phosphate-receptor-dependent sorting of cathepsin D to lysosomes. *Mol. Biol. Cell.* 19:2350–2362.

Puertollano, R., R.C. Aguilar, I. Gorshkova, R.J. Crouch, and J.S. Bonifacino. 2001. Sorting of mannose 6-phosphate receptors mediated by the GGAs. *Science.* 292:1712–1716.

Raussens, V., C.A. Fisher, E. Goormaghtigh, R.O. Ryan, and J.M. Ruysschaert. 1998. The low density lipoprotein receptor active conformation of apolipoprotein E. Helix organization in n-terminal domain-phospholipid disc particles. *J. Biol. Chem.* 273:25825–25830.

Robenek, H., S. Lorkowski, M. Schnoor, and D. Troyer. 2005. Spatial Integration of TIP47 and Adipophilin in macrophage lipid bodies. *J. Biol. Chem.* 280:5789–5794.

Schägger, H., W.A. Cramer, and G. von Jagow. 1994. Analysis of molecular masses and oligomeric states of protein complexes by blue native electrophoresis and isolation of membrane protein complexes by two-dimensional native electrophoresis. *Anal. Biochem.* 217:220–230.

Scott, G.K., H. Fei, L. Thomas, G.R. Medigeshi, and G. Thomas. 2006. A PACS-1, GGA3 and CK2 complex regulates CI-MPR trafficking. *EMBO J.* 25:4423–4435.

Seaman, M.N. 2004. Cargo-selective endosomal sorting for retrieval to the Golgi requires retromer. *J. Cell Biol.* 165:111–122.

Shevchenko, A., I. Chernushevic, M. Wilm, and M. Mann. 2002. "De novo" sequencing of peptides recovered from in-gel digested proteins by nano-electrospray tandem mass spectrometry. *Mol. Biotechnol.* 20:107–118.

Shiba, T., H. Takatsu, T. Nogi, N. Matsugaki, M. Kawasaki, N. Igarashi, M. Suzuki, R. Kato, T. Earnest, K. Nakayama, and S. Wakatsuki. 2002. Structural basis for recognition of acidic-cluster dileucine sequence by GGA1. *Nature.* 415:937–941.

Swamy, M., G.M. Siegers, S. Minguet, B. Wollscheid, and W.W. Schamel. 2006. Blue native polyacrylamide gel electrophoresis (BN-PAGE) for the identification and analysis of multiprotein complexes. *Sci. STKE.* 2006:pl4.

Tansey, J.T., A.M. Huml, R. Vogt, K.E. Davis, J.M. Jones, K.A. Fraser, D.L. Brasaemle, A.R. Kimmel, and C. Londos. 2003. Functional studies on native and mutated forms of perilipins. A role in protein kinase A-mediated lipolysis of triacylglycerols in chinese hamster ovary cells. *J. Biol. Chem.* 278:8401–8406.

Tauchi-Sato, K., S. Ozeki, T. Houjou, R. Taguchi, and T. Fujimoto. 2002. The surface of lipid droplets is a phospholipid monolayer with a unique fatty acid composition. *J. Biol. Chem.* 277:44507–44512.

Than, N.G., B. Sumegi, G. Than, G. Kispal, and H. Bohn. 1998. Cloning and sequence analysis of cDNAs encoding human placental tissue protein 17 (PP17) variants. *Eur. J. Biochem.* 258:752–757.

Than, N.G., B. Sumegi, S. Bellyei, T. Berki, G. Szekeres, T. Janaky, A. Szigeti, H. Bohn, and G.N. Than. 2003. Lipid droplet and milk lipid globule membrane associated placental protein 17b (PP17b) is involved in apoptotic and differentiation processes of human epithelial cervical carcinoma cells. *Eur. J. Biochem.* 270:1176–1188.

Tucker, J., G. Sczakiel, J. Feuerstein, J. John, R.S. Goody, and A. Wittinghofer. 1986. Expression of p21 proteins in *Escherichia coli* and stereochemistry of the nucleotide-binding site. *EMBO J.* 5:1351–1358.

Wessel, D., and U.I. Flugge. 1984. A method for the quantitative recovery of protein in dilute solution in the presence of detergents and lipids. *Anal. Biochem.* 138:141–143.

Wolins, N.E., B. Rubin, and D.L. Brasaemle. 2001. TIP47 Associates with lipid droplets. *J. Biol. Chem.* 276:5101–5108.

Xu, G., C. Sztalryd, X. Lu, J.T. Tansey, J. Gan, H. Dorward, A.R. Kimmel, and C. Londos. 2005. Post-translational regulation of adipose differentiation-related protein by the ubiquitin/proteasome pathway. *J. Biol. Chem.* 280:42841–42847.

Zhang, X.M., S. Ellis, A. Sriratana, C.A. Mitchell, and T. Rowe. 2004. Sec15 is an effector for the Rab11 GTPase in mammalian cells. *J. Biol. Chem.* 279:43027–43034.